

A Novel Compact Substrate Integrated Waveguide Filter Using Miniaturized Stepped Impedance Metamaterial Unit Cell

Zied Troudi¹, Jan Machac², and Lotfi Osman^{1, *}

Abstract—Novel substrate integrated waveguide bandpass filters are presented by using a complementary split-ring resonator. The proposed stepped impedance octagonal complementary split-ring resonator (SI-OCSR) presents high miniaturization compared to the classical octagonal complementary split-ring resonator (O-CSR). Additionally, two different filter configurations consisting of two cascaded cells with different coupling between the CSR are proposed. A comparison between the proposed filters and the other ones reported in the literature has proven the advantages of the proposed filters, namely compact size, high in-band return loss, and ease of integration. A good agreement between the simulated and measured results has been reached, which verifies the validity of the design methodology.

1. INTRODUCTION

Several technologies have been proposed by researchers to improve the performance of filters. The compactness, low insertion loss, high rejection level, and low cost are present a field of activity of fundamental interest. Substrate integrated waveguide (SIW) technology [1, 2] has provided attractive proprieties for the realization of filters and microwave devices. SIW technology offers several benefits like high-power handling capability, low radiation losses, and low fabrication cost of various RF components using SIW structures. This structure is synthesized by a dielectric layer, top and bottom ground planes and two rows of metallic via arrays of holes that are placed between these two planes. The main disadvantage of the SIW filter is large. To overcome these constraints, several solutions have been proposed by researchers [3–6]. In this context, metamaterials [7] have been widely studied for their potential to create new electromagnetic properties [8] and miniaturize RF circuits. The conception of RF circuits based on metamaterial will be more developed by using a different concept such as composite right/left-handed (CRLH) transmission line, SRR, and complementary split-ring resonator (CSR) [9–11]. In the field of filtering, the use of metamaterials allows having miniature structures and designing filters with highly interesting properties. Indeed, metamaterials are artificial materials, which have electromagnetic properties that are not accessible in nature, namely negative permittivity and permeability. Based on the duality concepts and Babinet principle [12], Falcone et al. introduced the first complementary split-ring resonator (CSR) [13] in 2004 as a new metamaterial resonator. Although the CSRs are considered as electric dipoles that can produce negative permittivity, their major advantage lies in their compact size, high rejection, and simplicity of fabrication.

In the first part, this paper focuses on developing a new compact CSR based on a stepped impedance technique. The proposed CSR is studied, and an equivalent circuit model is investigated by the even-odd mode method [14]. In the second part, a substrate integrated waveguide (SIW) bandpass filters loaded by stepped impedance octagonal CSR (SI-OCSR) are designed and fabricated.

Received 14 November 2020, Accepted 22 December 2020, Scheduled 3 January 2021

* Corresponding author: Lotfi Osman (lotfi.osman@supcom.tn).

¹ Microwave Electronics Research Laboratory: LR18ES43, Department of Physics, Faculty of Sciences of Tunis, University of Tunis El Manar, 2092, Tunisia. ² Department of Electromagnetic Field, Czech Technical University in Prague, Czech Republic.

The proposed filters operate in the UHF band. A significant improvement in the performance filters is achieved. Indeed, the good compactness (a total size equal to $l0.043\lambda_g^2$ and $0.017\lambda_g^2$ for type I and type II configurations, respectively), low loss, ease of fabrication, and ease of integration with other electrical circuits. The design details, simulated and experimental results are presented, described, and discussed.

2. SI-OCSRR DESIGN

Figure 1 represents the schematic view of a classical octagonal CSRR and the proposed stepped impedance octagonal CSRR. A modification of the conventional SIR has been introduced; triangularly shaped sections of the low impedance line are added to the classic O-CSRR. Both resonators are considered as resonant electric dipoles. They require an axial electric excitation to determine and compare the frequency responses and effective permittivities. Then, the electric field will be perpendicular to the plane of the metallization while the magnetic field will be parallel to it. Accordingly, both circuits are etched in the ground plane of a microstrip transmission line as shown in Figure 3.

The results of the frequency response and effective permittivity were determined by the CST simulator by applying the necessary condition limits [15]. The studied structures are designed by a

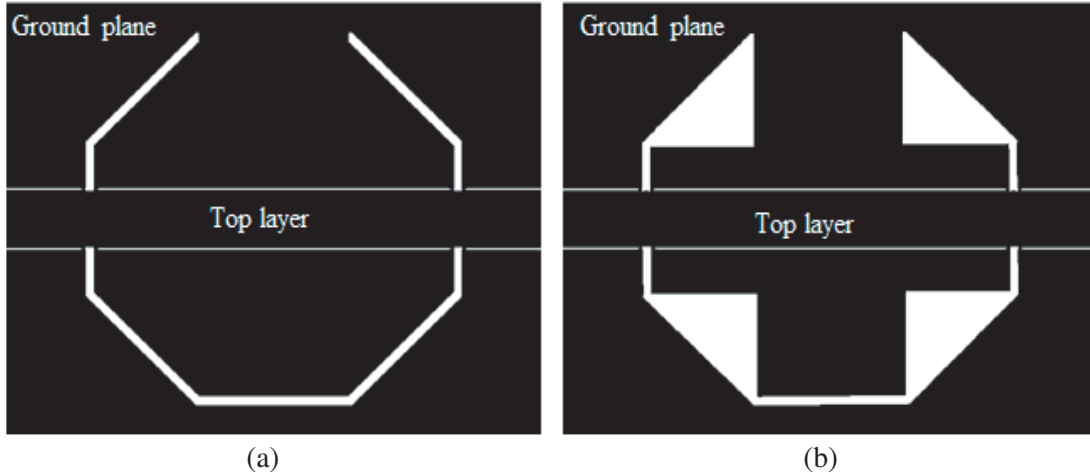


Figure 1. Micro-strip TL loaded with (a) conventional OCSRR, (b) SI-OCSRR.

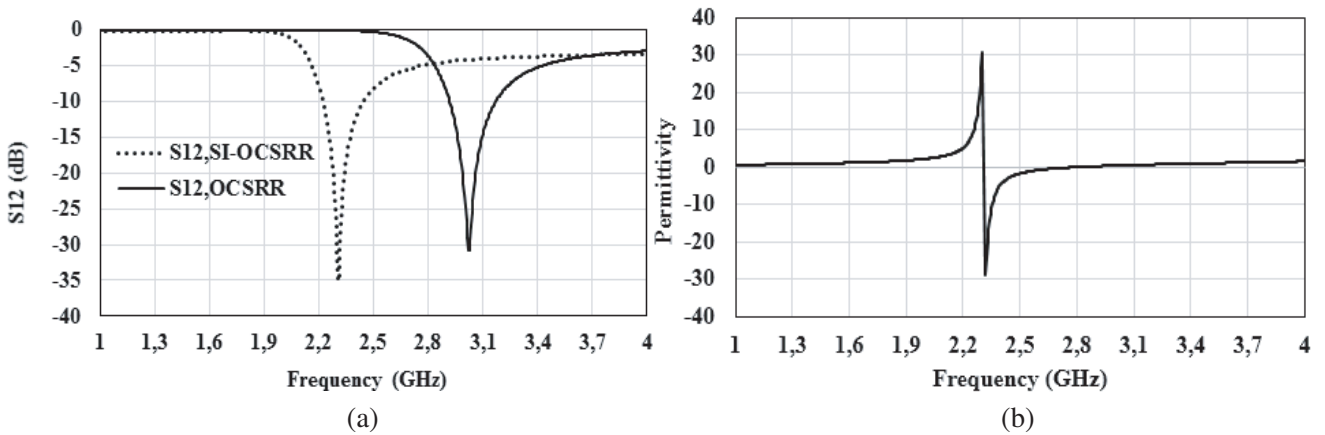


Figure 2. (a) Simulated transmission responses of OCSRR and SI-OCSRR. (b) Real part of the negative permittivity of the proposed CSRR.



Figure 3. Layout of SIW structure.

substrate Rogers RO3006 with a thickness of 0.762 mm and permittivity of 6.15.

Figure 2(a) shows the transmission coefficients of both CSRRs. The proposed CSRR has a lower frequency (2.3 GHz) than the conventional CSRR (3.02 GHz) for the same size of the physical circuit. Therefore, a miniaturization factor about 0.76 is achieved.

The real part of the effective permittivity for the proposed CSRR unit cell is determined from the simulated S -parameters. This real part of the permittivity takes a negative value around the resonant frequency, as depicted in Figure 2(b).

3. SIW CAVITY DESIGN

The proposed SIW cavity is illustrated in Figure 3. The waveguide cutoff frequency of the cavity SIW is calculated by Equation (6), and the effective width and length are determined by Equations (1) and (8), respectively [16].

$$f_0 = \frac{c_0}{2\sqrt{\epsilon_r}} \sqrt{\frac{1}{W_{eff}^2} + \frac{1}{L_{eff}^2}} \quad (1)$$

$$W_{eff} = w - 1.08 \frac{d^2}{p} + 0.1 \frac{d^2}{w} \quad (2)$$

$$L_{eff} = w - 1.08 \frac{d^2}{p} + 0.1 \frac{d^2}{l} \quad (3)$$

where c is the speed of light in vacuum, ϵ_r the relative permittivity, μ_r the relative permeability of the substrate, d the diameter of the SIW via, p the pitch (period), w the width of the cavity, and l the length of the cavity.

The physical characteristics of the microstrip line that represents the intermediate transition between the planar circuit and the SIW are mostly detailed in [17].

4. SIW BANDPASS FILTERS WITH SI-OCSRR

4.1. Reversely Side-by-Side Configuration (Type I)

The use of the evanescent-mode propagation concept [18] presents more advantages than other design techniques. Indeed, when a waveguide is loaded by electric dipoles, an additional passband below their cut-off frequency can be attained. On the other hand, the CSRR behaves like an electric dipole that can produce a negative effective permittivity. As a result, the CSRR requires an axial electric field excitation. Meanwhile, the electric field for the dominant mode (TE_{101}) of the SIW is perpendicular to the top and bottom plates. This arrangement guarantees that CSRR is properly excited when etching

in the top metallic surface. The position of the CSRR plays an important role in the behaviors of the frequency responses of the filter. For that reason, the reversely side-by-side configuration represents good filtering [18].

The configuration of the SIW bandpass filter structure loaded with classical octagonal CSRR is represented in Figure 4(a), and the configuration of the SIW bandpass filter loaded with stepped impedance octagonal shape CSRR is depicted in Figure 4(b).

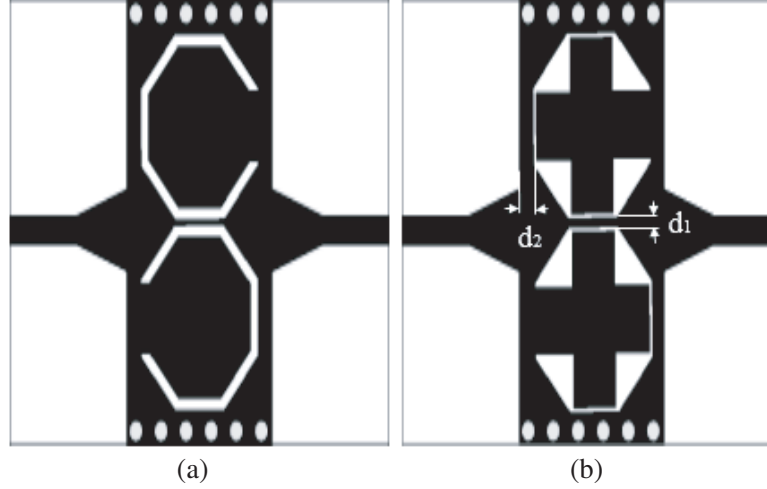


Figure 4. Configuration of the SIW bandpass filter loaded by (a) the classical octagonal CSRR, (b) the proposed octagonal CSRR.

According to the conventional filter design methodology, the external Q factors and coupling coefficients represent the most important factors which are determined by using the circuit synthesis of a low-pass prototype filter. Generally, the determination of the coupling coefficients is achieved from the following equation [19]:

$$K = \frac{f_1^2 - f_2^2}{f_1^2 + f_2^2} \quad (4)$$

where f_1 and f_2 denote the resonance frequencies of the low and high modes, respectively. The external Q factors can be evaluated using the following relation [19].

$$Q = \frac{2f_0}{\Delta f_{3\text{dB}}} \quad (5)$$

where f_0 represents the resonance frequency, and $\Delta f_{3\text{dB}}$ denotes the 3-dB bandwidth.

The elements of the circuit are defined by the metallic via which is indicated by an inductance L_v . Also, the equivalent circuit model of the SIR-CSRR is denoted by an inductance L_r and a capacitance C_r . The inductive and capacitive couplings between the SIW and CSRR are designated by L_c and C_c , respectively. The coupling between the two CSRRs is considered as a combination of the electrical and magnetic couplings. Thus, the coupling is modeled by C_s and L_s . The electric filter model is shown in Figure 5. The equivalent circuit parameters are obtained using matrix $ABCD$, as detailed in [19].

To facilitate the design procedure, Figures 6(a) and 6(b) represent the values of the coupling coefficients and external quality factors versus distances d_1 (the waveguide length between the CSRR and input microstrip) and d_2 (coupling distance between resonators) extract by Equations (4) and (5).

Figure 7 depicts the simulated response of the proposed filter with the new stepped impedance octagonal CSRR and electric circuit response. As can be seen, a good agreement is achieved between the CST and circuit model simulations.

Figure 8 shows the simulation results of the SIW bandpass filter loaded by classical CSRR and the SIW bandpass filter loaded by the proposed CSRR. While the resonance frequency occurs at 2.95 GHz,

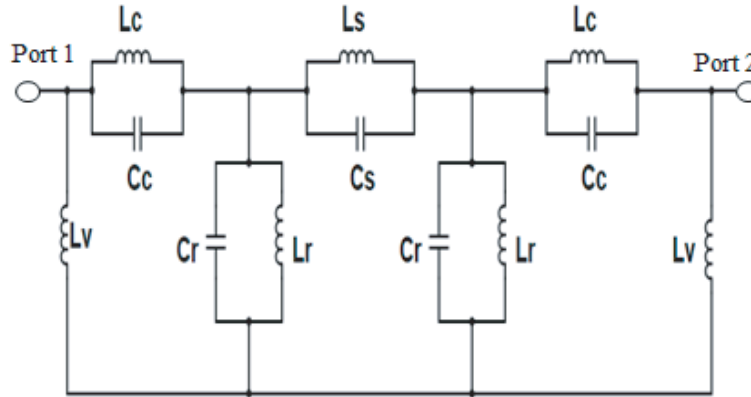


Figure 5. Equivalent circuit of the SIW bandpass filter loaded by CSRR side-by-side reversely configuration, (Lumped-element values are $L_v = 3.6$ nH, $C_r = 4.95$ pF, $L_r = 0.95$ nH, $C_c = 0.65$ pF, $L_c = 0.35$ nH, $L_s = 0.49$ nH, $C_s = 5.37$ pF).

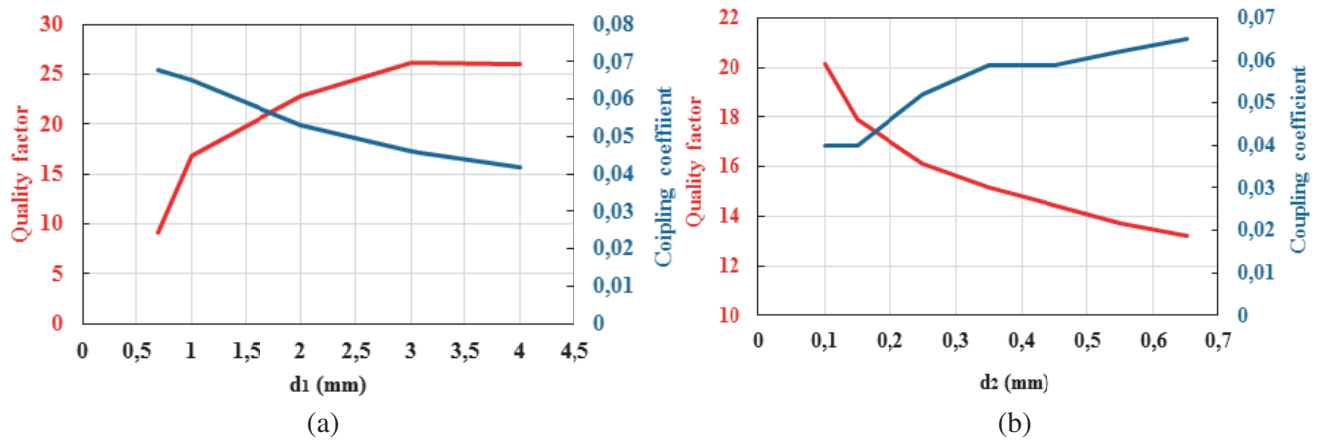


Figure 6. (a) External quality factor and coupling coefficient versus distance d_1 . (b) External quality factor and coupling coefficient versus distance d_2 .

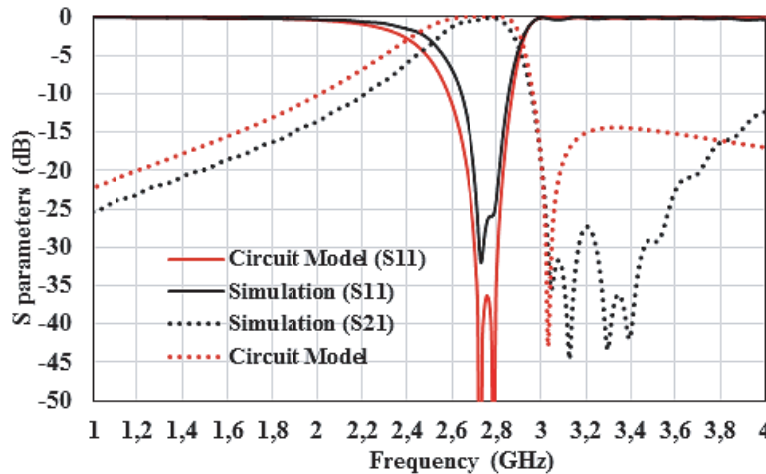


Figure 7. EM-simulated and circuit model S -parameters of SIW bandpass filter loaded by SI-OCSRR reversely side by side configuration. (The geometrical parameters are $w = 8.3$ mm, $l = 15.8$ mm, $d = 0.8$ mm, $P = 1.5$ mm, $d_1 = 0.86$ mm, $d_2 = 0.23$ mm).

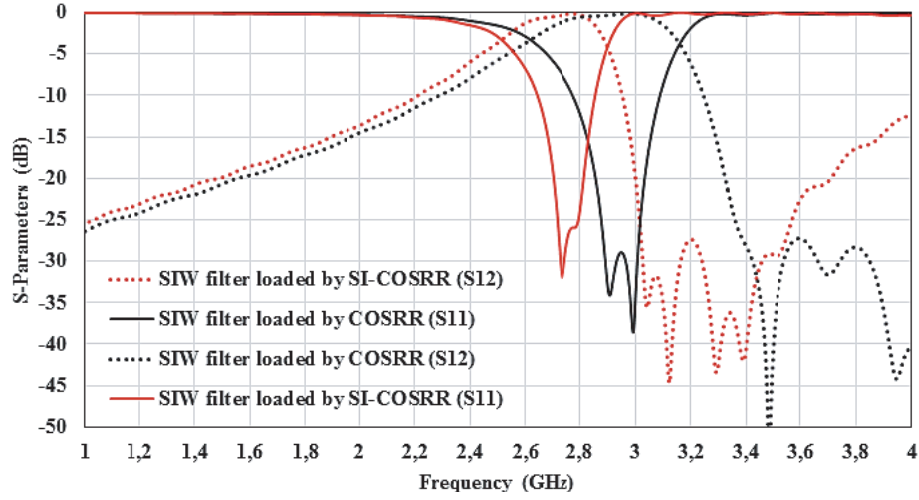


Figure 8. Simulated frequency responses of filter loaded by classical CSRR and filter loaded by proposed CSRR.

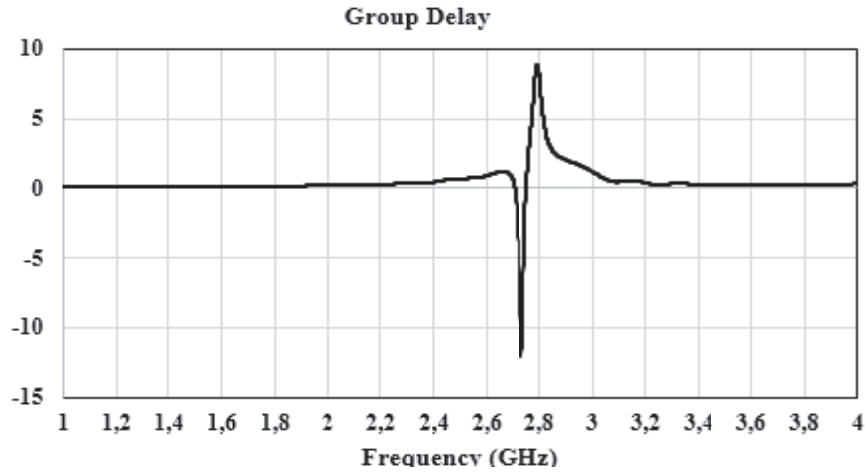


Figure 9. Group delay of the filter loaded by SI-OCSR (Type I).

a relative bandwidth is equal to 17%, and a low insertion loss of 0.14 dB is obtained. Thus, the total size is calculated at $0.050\lambda_g^2$ (146.16 mm^2), and a transmission zero is located in the upper band due to the dominant magnetic coupling created by via. It can be noticed that the resonance frequency of the designed SIW bandpass filters loaded by the proposed CSRR unit-cells has shifted by 0.2 GHz for the same size in comparison with the SIW bandpass filter loaded by the classical CSRR. Furthermore, the insertion loss has increased but is still low enough (0.27 dB). It is also observed that a relative bandwidth of 13% is reached. The bandwidth of the proposed filter can be controlled by changing the distance d_2 between the two SI-OCSR (changing mutual coupling). The bandwidth decreases when this distance is smaller because the magnetic coupling becomes easier when the CSRR is close to the center. However, a transmission zero is located in the upper band. The transmission zero is described by Equation (6). The transmission zero located below the first transmission zero is created by the mutual coupling. Figure 9 depicts the group delays of the proposed filter (type I).

$$f_z = \frac{1}{2\pi\sqrt{L_c C_c}} \quad (6)$$

4.2. Nested Configuration (Type II)

In this section, other arrangements of the proposed unit cell have been designed with the same dimensions as previous structures. The new bandpass SIW filter is shown in Figure 10(a). For this configuration, the asymmetrical plane can be used along the longitudinal direction. Thus, the same circuit model used in the previous section is exploited, except that the two CSRRs are modeled by one resonator (L_r , C_r). The simplified circuit model is shown in Figure 10(b). According to the equivalent-circuit model, L_c and C_c are used to describe the inductive and capacitive couplings between the resonators and the SIW structure, respectively. Therefore, the resonance frequency becomes lower because of increasing the total inductance L_r . Besides, the resonance frequency can be controlled by the physical size of the resonator. On the other hand, the bandwidth of the filter can be adjusted by changing the mutual inductive and capacitive couplings between the two CSRRs.

The results of the electromagnetic simulated and circuit model S -parameters are in good agreement as shown in Figure 11. A resonance frequency is located at 1.73 GHz, and a relative bandwidth is around 7%. Further, the in-band return loss is equal to 19.45 dB. Moreover, the insertion loss is at 0.96 dB, and the size of the filter is $0.017\lambda_g^2$ (146.16 mm^2). Also, a miniaturization factor of 0.59 has been achieved in comparison with the SIW bandpass filter loaded by the classical CSRR. The group delay of the proposed filter (Type II) is illustrated in Figure 12.

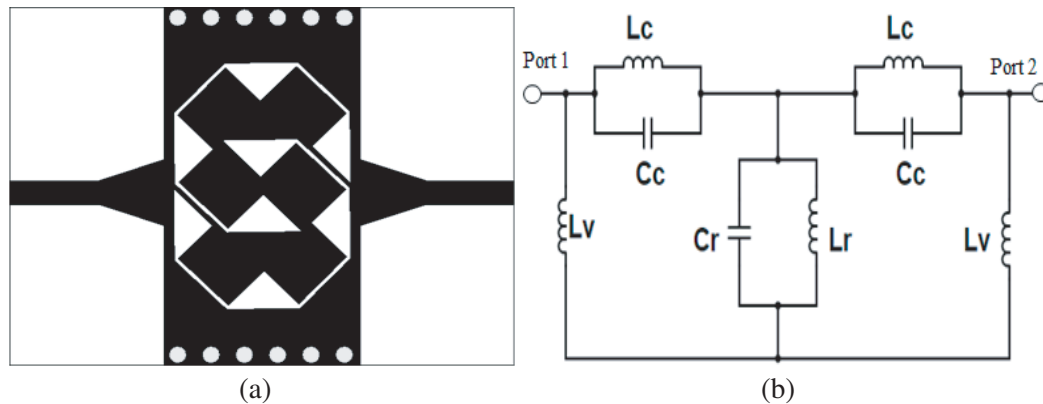


Figure 10. Configuration of the SIW bandpass filter loaded by proposed CSRR. (a) Equivalent circuit of the SIW bandpass filter loaded by CSRR nested configuration. (b) (Lumped-element values are $C_r = 6.1 \text{ pF}$, $L_r = 4.15 \text{ nH}$, $C_c = 1.55 \text{ pF}$, $L_c = 1.7 \text{ nH}$, $L_v = 1.95 \text{ nH}$).

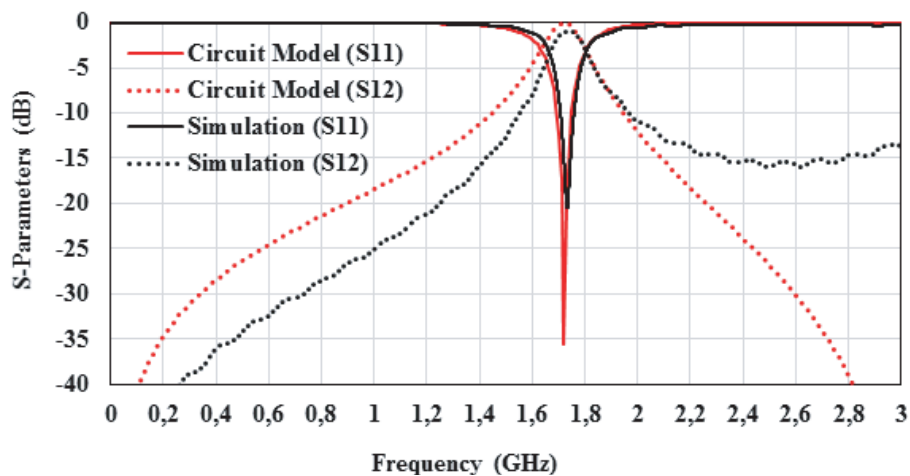


Figure 11. EM-simulated and circuit model S -parameters of SIW bandpass filter loaded by CSRR.

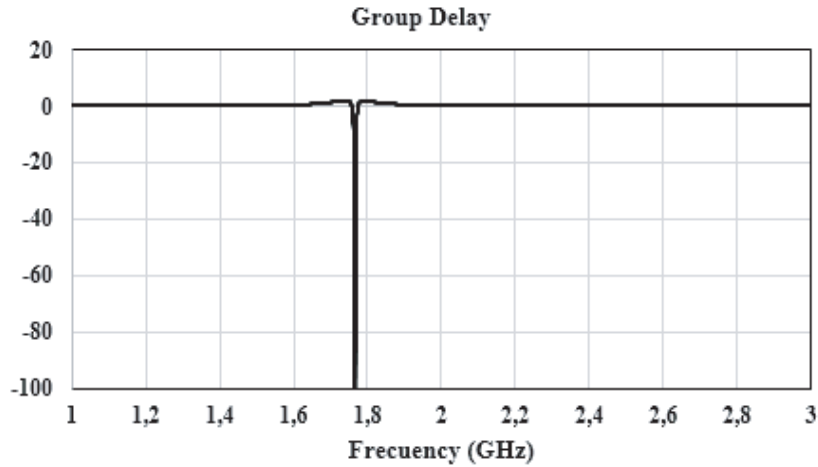


Figure 12. Group delay of the proposed filter loaded by SI-OCSRR (Type II).

4.3. Fabrication and Measurements

In this part, the designed SIW bandpass filters, such as the SIW bandpass filter loaded by classical CSRR, the SIW structure loaded by proposed CSRR with reversely side-by-side configuration (Type I), and with nested configuration (Type II), were designed, fabricated, and measured to confirm the simulated results. These filters are fabricated on a Rogers RO3006 substrate with a permittivity of 6.15 and thickness of 0.762 mm. The total size of the filters is 146.16 mm². The measured frequency response is characterized using a ZVA67 network analyzer. Figure 13 shows photographs of the fabricated filters.

Figure 14 shows the simulated and measured SIW bandpass filters loaded by the classical CSRR

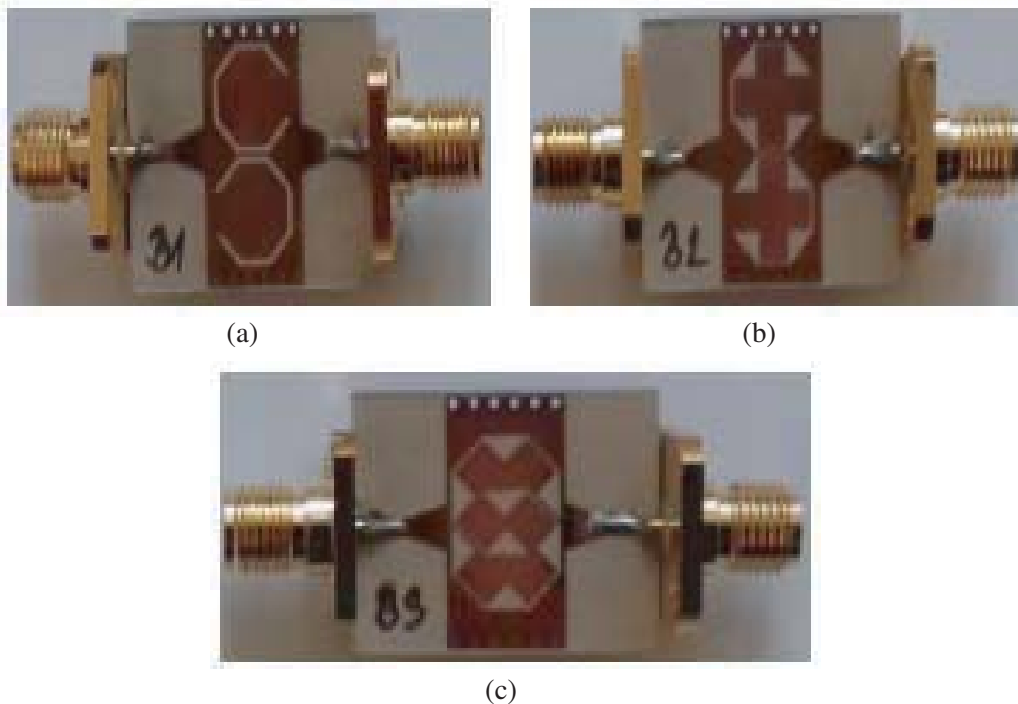


Figure 13. Photograph of the fabricated SIW bandpass filters loaded by (a) classical CSRR, (b) proposed CSRR (Type I), (c) proposed CSRR (Type II).

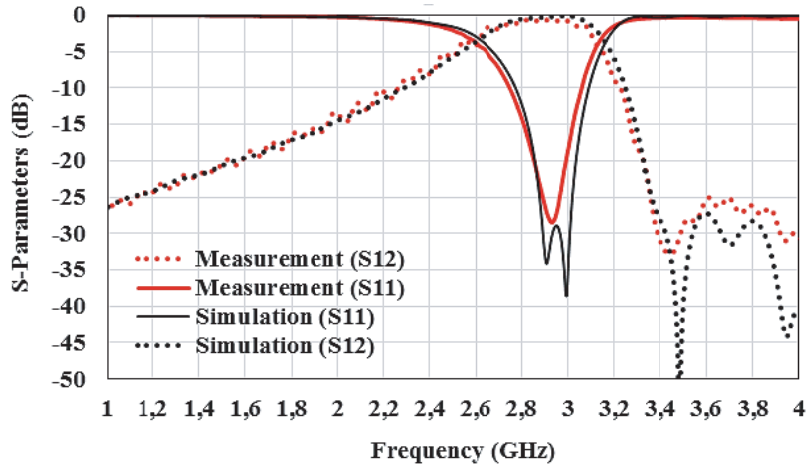


Figure 14. Simulated and measured frequency responses of the SIW filters bandpass loaded by the classical CSRR.

unit-cells. The comparison between the simulation and measurement results indicates a good agreement. The measured center frequency and 3-dB bandwidth are equal to 2.93 and 0.5 GHz, respectively. The insertion loss is approximately valued at 0.6 dB. Also, the measured return losses are better than 28 dB, and the measured stopband attenuation is nearly 20 dB (from 4.3 to 4.4 GHz).

Figure 15 shows a comparison between the simulated and measured frequency responses of the SIW filters loaded by the proposed CSRR with reverse side by side configuration (Type I). A good agreement between the measurement and simulation *S*-parameters is obtained. The measured resonance frequency and insertion loss are 2.73 GHz and 0.75 dB, respectively. The measured 3-dB bandwidth of the designed SIW filters is 0.4 GHz, and the measured return loss is better than 21 dB.

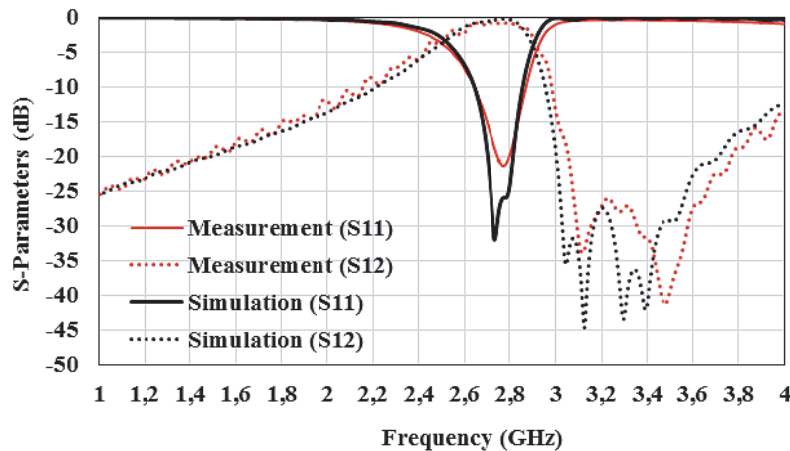


Figure 15. Simulated and measured frequency responses of the SIW bandpass filters loaded by the proposed CSRR with side by side reversely configuration.

The measured and simulated responses of the proposed SIW loaded by CSRR (type II) with the nested configuration are plotted in Figure 16. A good agreement between the measured and simulated results is achieved. The measured resonance frequency is found around 1.72 GHz, and the insertion losses are evaluated at 1 dB. The 3-dB bandwidth is equal to 0.1 GHz, and the measured return loss is 17.75 dB.

Table 1 summarizes the comparison between the simulated and measured results concerning the proposed filters.

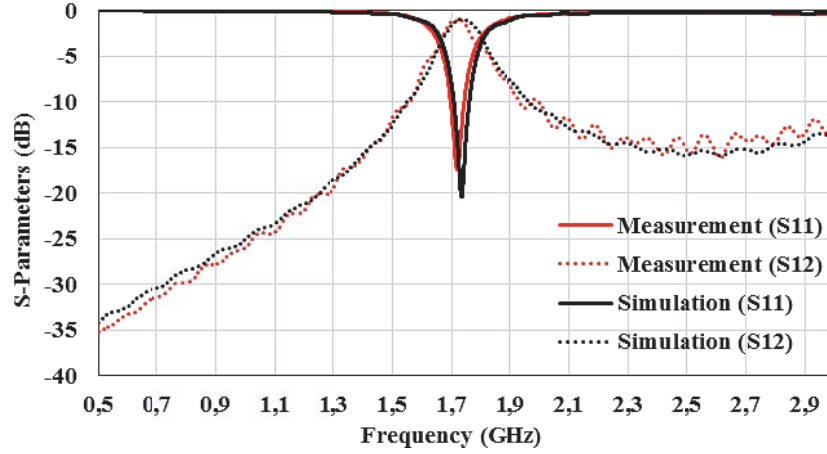


Figure 16. Simulated and measured frequency responses of the SIW bandpass filters loaded by the proposed CSRR with nested configuration.

Table 1. Comparison between the simulated and measured results.

		Conventional	Type I	Type II
Simulation	Fr (GHz)	2.95	2.75	1.73
	IL (dB)	0.14	0.27	0.95
	RL (dB)	28	25	19
	Size (λ_g^2)	0.050	0.043	0.017
Measure	Fr (GHz)	2.93	2.73	1.72
	IL (dB)	0.6	0.75	1
	Rl (dB)	20	21	17.75
	Size (λ_g^2)	0.050	0.043	0.017

The performances of the proposed type I and type II filters in terms of size, fractional bandwidth, insertion loss, and return loss are compared with other SIW bandpass filters reported in the literature and summarized in Table 2. Accordingly, it can be concluded that the filters suggested in this paper have good performances, namely compact dimension, insertion loss, and high in-band return.

Table 2. Comparison between the proposed structures and references.

references	RL (dB)	IL (dB)	FBW (%)	Size (λ_g^2)
[19]	15	1.6	11.2	0.08
[20]	18	1.5	9.7	0.049
[21]	12	4	5.2	0.248
[22]	20	1.9	7	0.0968
[23]	10	0.9	8.2	0.051
[24]	12	1.7	4.3	3.23
[25]	21	1.1	7.8	0.0552
Our work (Type I)	21	0.75	14.65	0.043
Our work (Type II)	17.75	1	5.7	0.017

5. TWO-STAGE SIW BANDPASS FILTER (TYPE III)

Based on the proposed structure with the nested configuration, two pairs of identical unit cells are used to design a two-stage SIW bandpass filter. The proposed filter is described in Figure 17. Therefore, the distance L between the two resonators can be adjusted to obtain the desired coupling.

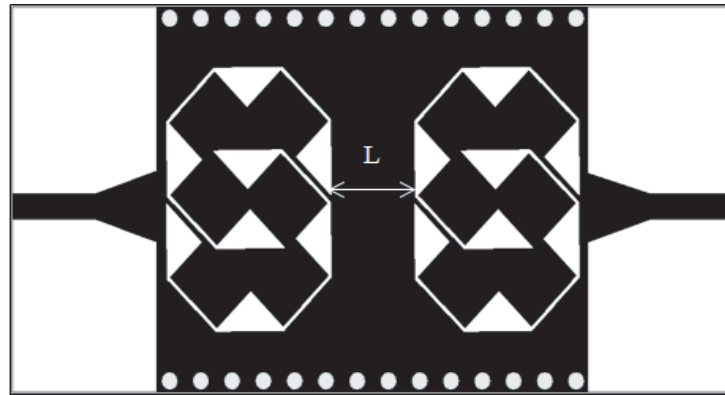


Figure 17. Layout of the proposed two-stage SIW bandpass filters loaded by proposed CSRR.

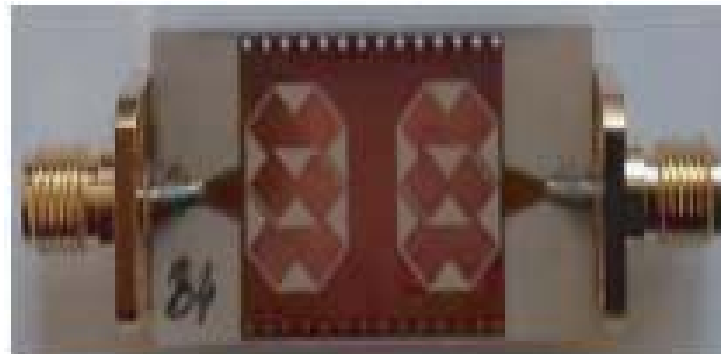


Figure 18. Photograph of the fabricated two-stage SIW bandpass filters using proposed CSRR with nested configuration.

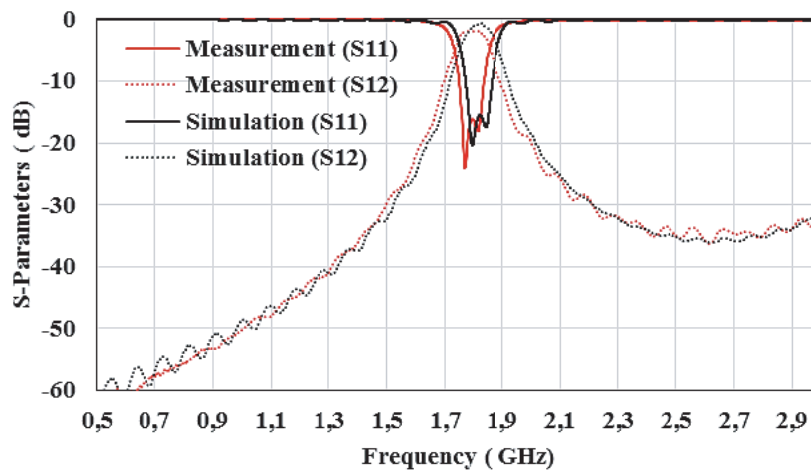


Figure 19. Simulated and measured frequency responses of the tow stage SIW bandpass filters loaded by the proposed CSRR with nested configuration.

Figure 18 shows a photograph of the two-stage SIW bandpass filter. Rogers RO 3006 with a permittivity of 6.15 and thickness of 0.762 mm is used as a substrate. The simulation results are attained by using CST software, and the measurement results are achieved by using a ZVA67 network analyzer.

Figure 19 shows the simulated and measured S -parameters of the two-stage filter, where a good agreement is achieved. The simulated resonance frequency and 3-dB bandwidths are 1.83 GHz and 0.102 GHz, respectively. The insertion loss is approximately 0.75 dB while the simulated return loss is 15.4 dB. Moreover, two transmission poles are obtained. For measurement results, two transmission poles in the pass bandwidth with a central frequency of 1.8 GHz are achieved. The measured 3-dB bandwidth of the projected filter ranges from 1.7 to 1.81 GHz, and its return loss is better than 15.5 dB. The measured insertion loss in the pass-band is 1.9 dB, and a measured stop-band rejection is observed in the upper band of 20 dB across a range from 1.6 up to 3.3 GHz.

6. CONCLUSION

In this paper, a novel miniaturized metamaterial unit cell is proposed using the stepped impedance technique. The electric dipole nature of the proposed CSRR is applied to obtain a bandwidth below the SIW cutoff frequency. This bandwidth is located below the waveguide cutoff frequency of the SIW. The compact SIW bandpass filters are presented by etching the CSRR on the metal cover of the SIW structure, where a downward frequency shift is acquired. Two configurations of the stepped impedance octagonal CSRR, namely reversely side-by-side and nested configuration, are suggested to ameliorate the size and performance of SIW filters. The designed SIW bandpass filters are fabricated and measured, and a good agreement between the simulated and measured results is achieved. The proposed filters have numerous advantages, such as compact size in comparison with the other SIW bandpass filters, ease of integration, small insertion loss, and high selectivity with improved stop-band rejection.

REFERENCES

1. Wu, G. K., D. Deslandes, and Y. Cassivi, "The substrate integrated circuits — A new concept for high-frequency electronics and optoelectronics," *6th International Conference on Telecommunications in Modern Satellite, Cable and Broadcasting Service, 2003, Telsiks 2003*, Vol. 1, P-III, IEEE, 2003.
2. Wu, K., "Integration and interconnect techniques of planar and non-planar structures for microwave and millimeter-wave circuits-current status and future trend," *Microwave conference, 2001, APMC 2001*, Vol. 2, 411–416, IEEE, Asia-Pacific, 2001.
3. Grigoropoulos, N., B. Sanz-Izquierdo, P. R. Young, et al., "Substrate Integrated Folded Waveguides (SIFW) and filters," *IEEE Microwave Wireless Compon Lett.*, Vol. 15, No. 12, 829–831, 2005.
4. Rong, Y., K. A. Zaki, M. Hageman, D. Stevens, and J. Gipprich, "Low-Temperature Cofired Ceramic (LTCC) ridge waveguide bandpass chip filters," *IEEE Trans. Microwave Theory Techn.*, Vol. 47, No. 12, 2317–2324, 1999.
5. Wang, Y., W. Hong, Y. Dong, B. Liu, H. J. Tang, J. Chen, et al., "Half Mode Substrate Integrated Waveguide (HMSIW) bandpass filter," *IEEE Microwave Wireless Compon. Lett.*, Vol. 17, No. 4, 265–267, 2007.
6. Moitra, S. and P. S. Bhowmik, "Modelling and analysis of Substrate Integrated Waveguide (SIW) and Half-Mode SIW (HMSIW) band-pass filter using reactive longitudinal periodic structures," *AEU — Int. J. Electron. Commun.*, Vol. 70, No. 12, 2016, 1593–1600.
7. Veselago, V. G., "The electrodynamics of substances with simultaneously negative values of ϵ and μ ," *Soviet Physics USPEKHI*, Vol. 10, No. 14, 509–514. January–February 1968.
8. Solymar, L. and E. Shamonina, *Waves in Metamaterials*, University Press.
9. Keshavarz, S. and N. Nozhat, "Dual-band Wilkinson power divider based on composite right/left-handed transmission lines," *2016 13th International Conference on Electrical Engineering/Electronics, Computer, Telecommunications and Information Technology (ECTI-CON)*, IEEE, 2016.

10. Keshavarz, S., et al., "Design and implementation of low loss and compact microstrip triplexer using CSRR loaded coupled lines," *AEU — International Journal of Electronics and Communications*, Vol. 111, 152913, 2019.
11. Karthikeyan, S. S. and R. S. Kshetrimayum, "Harmonic suppression of parallel coupled micro-strip line band-pass filter using CSRR," *Progress In Electromagnetics Research Letters*, Vol. 7, 193–201, 2009.
12. Falcone, F., T. Lopetegi, M. Laso, J. Baena, J. Bonache, M. Beruete, et al., "Babinet principle applied to the design of meta-surfaces and metamaterials," *Phys. Rev. Lett.*, Vol. 93, No. 1, 97401, 2004.
13. Falcone, F., T. Lopetegi, J. D. Baena, R. Marques, F. Martin, and M. Sorolla, "Effective negative-epsilon stopband microstrip lines based on complementary split-ring resonators," *IEEE Microw. Wireless Compon. Lett.*, Vol. 14, No. 6, 280–282, June 2004.
14. Crnojević-Bengin, V., (Ed.), *Advances in Multi-band Microstrip Filters*, Cambridge University, 2015.
15. Pendry, J. B., D. Schurig, and D. R. Smith, "Controlling electromagnetic fields," *Science*, Vol. 312, 1780–1782, 2006.
16. Nwajana, A. O., A. Dainkeh, and K. S. K. Yeo, "Substrate Integrated Waveguide (SIW) bandpass filter with novel microstrip-CPW-SIW input coupling," *Journal of Microwaves. Optoelectronics and Electromagnetic Applications*, Vol. 16, No. 2, 393–402, 2017.
17. Deslandes, D., "Design equations for tapered microstrip-to-substrate integrated waveguide transitions," *2010 IEEE MTT-S International Microwave Symposium*, 2010.
18. Dong, Y. D., T. Yang, and T. Itoh, "Substrate integrated waveguide loaded by complementary split-ring resonators and its applications to miniaturized waveguide filter," *IEEE Trans. Microw. Theory Tech.*, Vol. 57, No. 9, 2211–2223, 2009.
19. Pozar, D. M., *Microwave Engineering*, 3rd Edition, Chapter 8, Wiley, Hoboken, NJ, 2005.
20. Huang, L., I. D. Robertson, W. Wu, and N. Yuan, "Substrate integrated waveguide filters with broadside-coupled complementary split-ring resonators," *IET Microwaves, Ante. Propagat.*, Vol. 7, No. 10, 795–801, 2013.
21. Yan, T., X.-H. Tang, Z.-X. Xu, and D. Lu, "A novel type of band-pass filter using complementary open-ring resonator loaded HMSIW with an electric cross-coupling," *Microwave Opt. Technol. Lett.*, Vol. 58, No. 4, 998–1001, 2016.
22. Delmonte, N., L. Silvestri, M. Bozzi, and L. Perregri, "Compact half-mode SIW cavity filters designed by exploiting resonant mode control," *Int. J. RF Microwave Comput.-Aided Eng.*, Vol. 26, 72–79, 2016.
23. Azad, A. R. and A. Mohan, "Sixteenth-mode substrate integrated waveguide bandpass filter loaded with complementary split-ring resonator," *Electron. Lett.*, Vol. 53, No. 8, 546–547, 2017.
24. Chu, P., W. Hong, M. Tuo, K.-L. Zheng, W.-W. Yang, F. Xu, and K. Wu, "Dual-mode substrate integrated waveguide filter with flexible response," *IEEE Trans. Microw. Theory Tech.*, Vol. 65, No. 3, 824–830, 2017.
25. Danaeian, M. and K. Afrooz, "Compact metamaterial unit-cell based on stepped-impedance resonator technique and its application to miniaturize substrate integrated waveguide filter and diplexer," *International Journal of RF and Microwave Computer-Aided Engineering*, Vol. 29, No. 2, e21537, 2019.